Computers and Electronics in Agriculture 177 (2020) 105690

Contents lists available at ScienceDirect

Computers and Electronics in Agriculture

journal homepage: www.elsevier.com/locate/compag

Electrical impedance and image analysis methods in detecting and measuring Scots pine heartwood from a log end during tree harvesting

Antti Raatevaara[a,b,*], Heikki Korpunen[c], Markku Tiitta[d], Laura Tomppo[d], Sampo Kulju[c], Jukka Antikainen[e], Jori Uusitalo[a]

[a] Department of Forest Sciences, University of Helsinki, Latokartanonkaari 7, 00014 Helsinki, Finland
[b] Natural Resources Institute Finland, Latokartanonkaari 9, 00790 Helsinki, Finland
[c] Natural Resources Institute Finland, Korkeakoulunkatu 7, 33720 Tampere, Finland
[d] Department of Applied Physics, University of Eastern Finland, Yliopistonranta 1, 70210 Kuopio, Finland
[e] Natural Resources Institute Finland, Yliopistokatu 6, 80100 Joensuu, Finland

ARTICLE INFO

Keywords:
Scots pine heartwood
Image analysis
Region growing
KNN-matting
Electrical impedance

ABSTRACT

Scots pine (*Pinus sylvestris* L.) heartwood is naturally durable wood material which has not been fully utilized in the wood industry. Currently, there are no practical measurement methods for detecting and measuring heartwood in a tree harvesting. The objective of this study was to evaluate the applicability of an electrical impedance spectroscopy and an image analysis of a log end face for pine heartwood measurements from the harvesting perspective. Both methods were tested with a fresh wood material which was collected during the harvesting operations. The results indicate that both methods have potential to measure the heartwood from processed stems with an average heartwood diameter error being less than two centimeters for each method. However, the image analysis of the log end face is only appropriate when visible contrast between the heartwood and a sapwood exists. Our findings indicate that the studied heartwood detection methods show great potential in measuring the heartwood of the stem in the harvesting phase which would ideally benefit later links in wood value chains.

1. Introduction

The forestry sector is one of the most significant branches of industry in Finland. According to statistics, the forest sector equals 20 percentages of the export revenues in Finnish national economy (Natural Resources Institute Finland, 2019). The forest industry paid 2.2 billion Euro stumpage earnings to forest owners in 2017, and roughly 70% of the stumpage earnings are paid for sawlogs. Nationally, Scots pine (*Pinus sylvestris* L.) is the second most important tree species to Finnish forest industry only after Norway spruce (*Picea abies* L. Karst.). The Scots pine is also recognized as one of the most important sources of wood raw material elsewhere in Eurasia.

Scots pine sawn lumber is very versatile and can be utilized in both internal and external cladding of wooden structures. In the case of Scots pine, as with many other coniferous trees, a heartwood is naturally more durable material than a sapwood (Harju et al., 2003). This is mainly due to the chemical compounds in the heartwood. A formation of heartwood can be mostly explained with a cambial age of the tree at studied tree height (Uusitalo, 2004). When the tree ages, cells near the pith die and their properties may change significantly. The tree cells start to deposit extractives which include compounds such as terpenes, phenolic compounds and resins (Nascimento et al., 2013). The phenolic compounds are found to be natural preservatives against fungi that are deteriorating the wood (Nagy et al., 2006; Royer et al., 2012). According to Arshadi et al. (2013) the Scots pine heartwood contains up to five times the extractive concentration of the sapwood. The extractives generate color difference between the heartwood and the sapwood on a cross-sectional surface of tree which means that the heartwood can be visually detected. Additionally, the heartwood can be detected from the sapwood by measuring the moisture content of wood (e.g. Rust, 1999).

A modern wood value chain begins from the forest where the trees are felled, delimbed, and cross-cut into logs with cut-to-length (CTL) harvesters. In CTL harvesting, machine operators do the tree bucking by deciding the cross-cut points of each log with an assistance of harvester information system. A stem taper is measured automatically during the logging and the on-board computer calculates the most profitable log combination. The bucking is based on only external and visual measurements and subjective estimations of the wood properties, such as

* Corresponding author at: Department of Forest Sciences, University of Helsinki, Latokartanonkaari 7, 00014 Helsinki, Finland.
E-mail address: antti.raatevaara@helsinki.fi (A. Raatevaara).

https://doi.org/10.1016/j.compag.2020.105690
Received 14 November 2019; Received in revised form 31 July 2020; Accepted 31 July 2020
Available online 11 August 2020

dimensions, indications of decay, sweep, branches or knots. The internal properties of the trees are not considered mostly because there are no practical measurement equipment and methods available. Currently, the heartwood of a log is measured at sawmills with X-ray scanners. However, in the CTL harvesting the tree bucking decisions have already been made in the forest and the raw material can never be fully utilized. In order to maximize the value of heartwood, novel methods are needed to support the harvesting decision making.

The findings of Björklund (1999) indicate that the amount of Scots pine heartwood varies significantly between both stands and individual trees. Therefore, a reliable pre-harvesting prediction of the heartwood content is difficult and only after a robust detection of the heartwood the wood raw material optimization can be done efficiently. Nowadays, the pre-harvest single-tree measurements are not generally considered as cost-effective and the single-tree information could be easily lost between the measurement and the actual harvesting. Thus, the heartwood content should be measured during the harvesting process, as early as possible in the wood value chain.

Electrical impedance spectroscopy (EIS) is quite a novel method for characterizing and imaging the electrical properties of materials (Barsoukov and Macdonald, 2005). With the electrical impedance spectroscopy method, electrodes are used to create dynamic electric field in the wood, measure the complex electrical impedance and determine the properties of wood material in the effective electric field. The results may be utilized in the further processing, making it possible to classify the wood according to its properties.

EIS has been applied to wood research and various properties of wood have been widely studied (Zelinka et al., 2008; Tomppo et al., 2011; Tiitta et al., 2020). In addition, by combining EIS with other measurement methods, more accurate analyzes of the wood have been achieved (Tiitta et al., 2017).

The extractives of Scots pine heartwood have a significant effect on electrical properties and it can be analyzed using electrical impedance spectroscopy (Tiitta et al., 2003; Tiitta, 2006; Tomppo et al., 2011). The correlation is clear both in a fresh and dried wood. According to the earlier studies, resin acid content (and decay resistance) may be determined using electrical impedance spectroscopy.

The bottom end of cross-cut stem reveals a narrow view to the wood properties. This data could be captured with a RGB-camera installed to the harvester head and further analyzed with machine vision algorithms to guide the bucking optimization of the stems. In the past studies, the focus of log end face image analysis has been on pith localization (Norell and Borgefors, 2008; Gazo et al., 2020), counting of annual rings (e.g. Norell, 2011) and biometric log traceability (Schraml et al., 2015). An automatic segmentation of the heartwood from the log end face image has received less attention, although it holds premise to improve bucking of stems in CTL-harvesting. However, the visual disparity between the heartwood and the sapwood is not only species-dependent but also relative to the season when the tree is harvested.

The aim of this study was to test and compare two novel methods, electrical impedance spectroscopy and image analysis for measuring the dimensions of Scots pine heartwood of bottom ends of fresh harvested logs.

2. Material and methods

The applicability of both EIS and image analysis measurements was tested with a wood material received from typical Finnish tree harvesting sites. The material collection and analyses were conducted in such ways that the harvesting and forwarding work was disturbed as little as possible and the harvesting work safety regulations were followed.

2.1. Stand selection and pre-harvest measurement

The Scots pine stems were collected from two harvesting sites in June 2017 in Central Western Finland. Generally, the sites were located on average mineral soils that were estimated to represent average fertility of pine stands in Finland. The first and second sites were evaluated to be blueberry type (MT), and the third was lingonberry type (VT). The stems were randomly selected from the center of each site in order to avoid possible influences from neighbor sites. The selected stems were measured and marked prior to the harvesting.

Table 1
The descriptions of the sample stands with mean stem diameter at breast height (dbh), height, height to crown base, age, amount of logs per tree measured with image analysis and EIS (N). Crown base height was measured as the distance between the stem bottom and the lowest living branch of the tree crown.

Stand	dbh (cm)	Height (m)	Crown height (m)	Age	N	
					Image	EIS
1	37.7	25.6	15.4	107	40	–
2	31.2	24.8	15.7	102	28	18
3	26.4	20.8	10.9	98	18	15

The pre-harvest measurement indexes were diameter at breast height (dbh), starting height of living crown and the total height of the tree. The diameter at breast height was measured by two cross-sectional measurements done with a tree caliper and the height was measured with electronic hypsometer (Vertex III-60). The selected stems were bucked and cross-cut into logs by a CTL harvester. The number of logs per stem varied from two to four and the variation in the log sample count per stem was caused by the dimensions, and visual properties of stems in relation to harvested log classes. The average tree and log descriptions of both test sites are presented in Table 1. Tree ages were estimated from the log end face images.

2.2. Image analysis, experimental measurements and statistical analysis of results

To compare the EIS and the image analysis method, both the heartwood ratios and absolute heartwood diameters were calculated. The bark of a tree was excluded from the measurements.

The practical section of the study consisted of four parts: post-harvesting activities on logging site, image analysis, experimental measurements and data analysis (Fig. 1). Detailed descriptions of each main part are presented in following sections.

2.3. Post-harvesting activities on logging site

The logs were photographed from the bottom ends after the harvesting in a daylight and within three hours from felling. The images were taken with Nikon D7200 camera equipped with a Sigma 17–50 mm f/2.8 EX DC OS HSM objective. A measurement bar was held as a reference on the parallel level with the log end face, and each log was identified with a number tag (Fig. 2a). Total of 86 log end face images were chosen for further analysis based on the visual contrast between the heartwood and the sapwood. Cases where the heartwood was not distinguishable with a bare eye, were excluded from the analysis.

For the EIS analysis, several centimeters thick discs were cross-cut from the bottom ends of 33 randomly selected logs. Thus, the same log ends where the heartwood could be visually detected (22) were utilized for both the image analysis and EIS. The discs were wrapped in a plastic to prevent the evaporation of water and extractives from the wood, and transported to a laboratory. The south position was marked on the stem surface before harvesting the tree.

2.4. Heartwood segmentation of the images

The images taken from the bottom end of each log (Fig. 2a) were

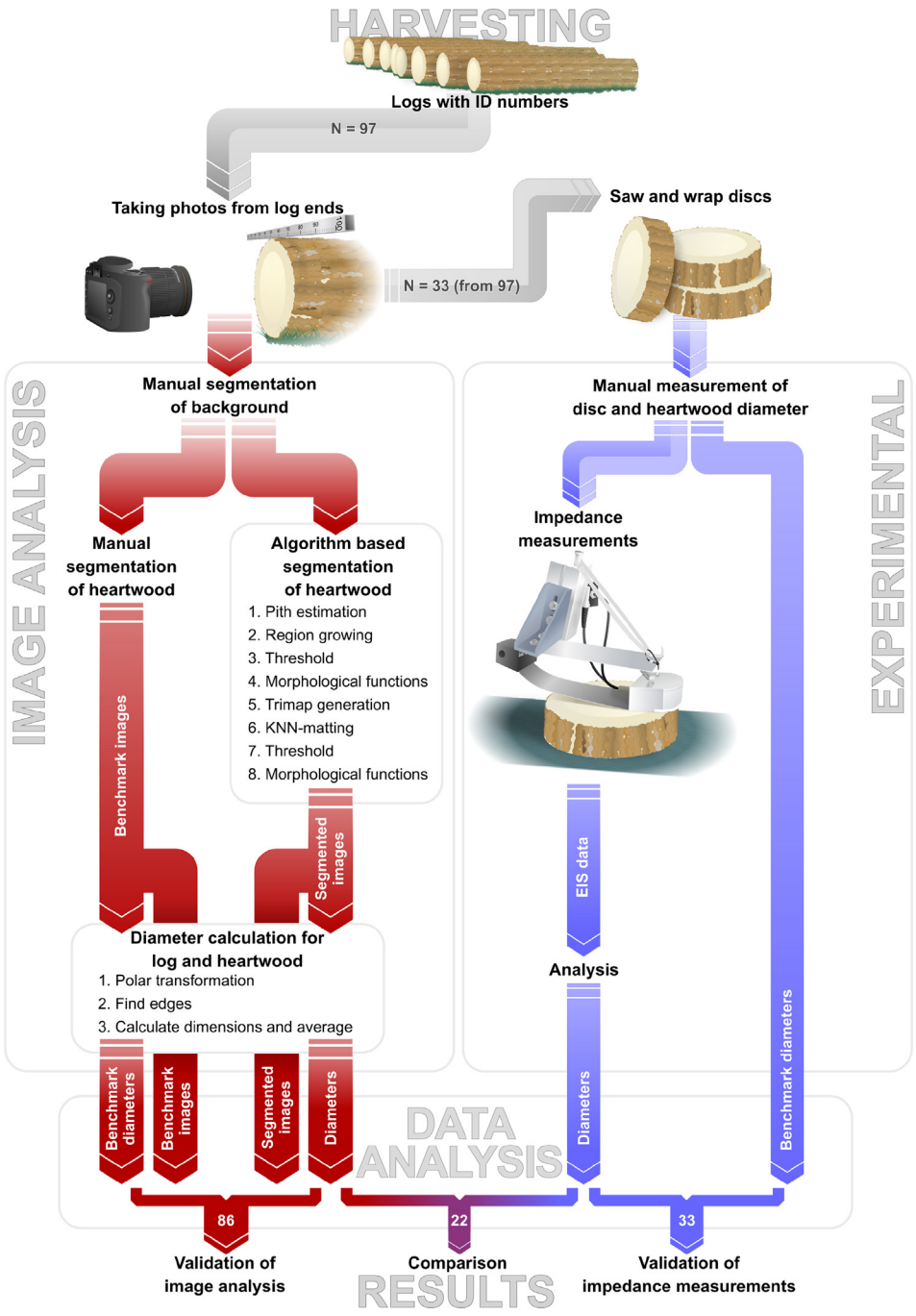

Fig. 1. Thematic flow chart of the manual, image analysis and impedance measurement study setup.

manually removed from the background with an open-source software "GIMP" (https://www.gimp.org) (Fig. 2b). These images were given as an input for the heartwood segmentation algorithm, which begins by locating the pith inside the heartwood. The segmentation was performed in two phases (Sections 2.4.1, and 2.4.2), where the heartwood region was first detected with a region growing method and later fine-tuned with k nearest neighbour image matting. The heartwood regions produced by the algorithm were finally compared to the

Fig. 2. A log end face image with measurement bar and ID-tag (**a**), log end face manually separated from the background (**b**), and manually segmented heartwood and sapwood (**c**).

ground-truth segmentations (Fig. 2c), which were manually drawn in the GIMP software.

2.4.1. Locating the pith and the use of confidence connected region growing to detect the heartwood

The image segmentation algorithm proposed in this study assumes that pixels located close to the pith form a continuous heartwood region with rather homogeneous values. On contrary, the pixels positioned between the edge of the log end face and previously described region, form a segment which pixel values have a lower intensity in grayscale-image than the pixels near the pith. The heartwood segmentation algorithm partitions these regions according to their color while utilizing an unsupervised, seeded region growing algorithm from open-source image processing library: Insight Segmentation and Registration Toolkit (SimpleITK) (Lowekamp et al., 2013).

The segmentation of the heartwood region begun with a localization of the pith from the log end face image. The used method to find the pith from the log end face assumes that annual growth rings are arranged as concentric circles around the pith. Orientations of the annual rings were estimated with a moving window (180 px × 180 px) in a HSV color space and Fast Fourier Transform (FFT). In FFT power spectrum of the annual rings, a vector pointing the position of pith was extracted as a first component of principal component analysis (PCA). The pith position estimate was calculated as an average position of the intersections made by the first components of PCA calculated from window images (Fig. 3a).

To enhance the contrast between the heartwood and the sapwood, the RGB-image (Fig. 2b) was converted into a HSV and CIE Lab color spaces. A highest contrast between the mentioned regions was achieved by an average from a saturation channel of the HSV and a first chrominance component (*a) of the CIE Lab color space image. The average intensity of these channels established the input image for the confidence connected region growing algorithm. A random noise on the log end face (e.g. scratches from saw chain or barkdust) was reduced with a median filtering of OpenCV-library (Bradski, 2000). The image resolution was also reduced to 1500 × 1000 pixels for faster computation.

A selection of seed-points for the confidence connected region growing was made according to the estimated position of pith. Seed-points were selected from nine squares which middle point was the estimated pith (Fig. 3b). The size and distance between the square plots was adjusted by the size of the log bottom end: square side and distance between each other was shorter on the smaller logs and correspondingly longer on the larger logs.

The confidence connected region growing was executed for several hundreds of seed-points depending on the size of log. These seed-points were sampled from the squares placed on the estimated heartwood region, where the growing of heartwood region was decided by neighboring pixel values and their participation (p) to the heartwood region was determined through formula defined as

$$\mu - c\sigma < p < \mu + c\sigma, \quad (1)$$

where μ is an average intensity of the region and σ is standard deviation of gray intensity values in the region. Predefined parameter c is a growing criterion.

The proposed heartwood regions of each region growing process were summed into a stack of images which was divided by the total count of images. The resulting average heartwood region (Fig. 3c) represents how many times each image pixel has been included into proposed heartwood region. Thus, a pixel has a high probability to be part of heartwood region if it has been part of the region in high proportion of the individual region growing processes.

The split between the heartwood and the sapwood regions was accomplished by setting threshold value on the grayscale image. An entropy-based approach called “MaximumEntropy” from ITK-library (Lowekamp et al., 2013) was chosen for the threshold method which is based on the variance in the pixel values: threshold maximizes the entropy within white and black pixels (Kapur et al., 1985).

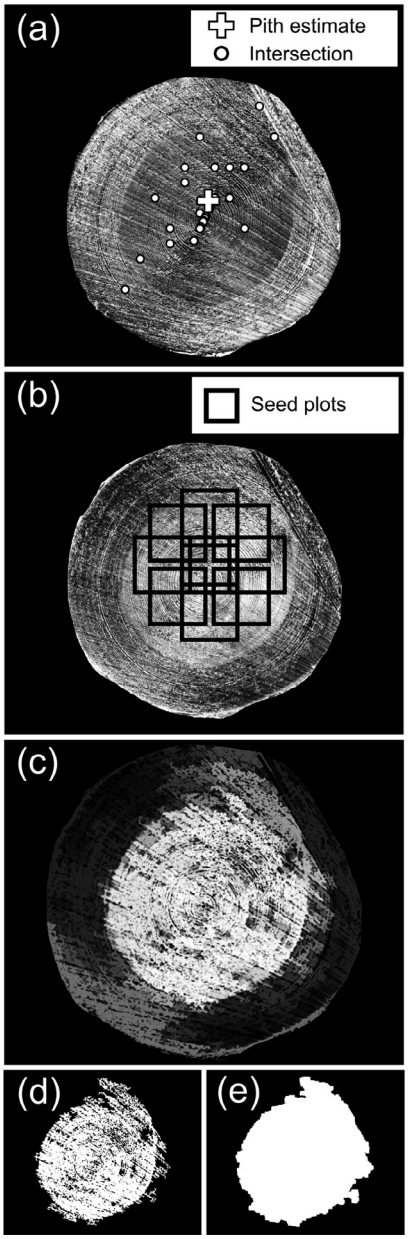

Fig. 3. Steps of the heartwood segmentation: (**a**) Pith localization, (**b**) Selection of seed-points, (**c**) An average region growing segmentation (**d**) Maximum entropy threshold of the image (**e**) The heartwood segment after a morphological functions.

In the binary image (Fig. 3d), the white segment represents the estimated heartwood region. As the last step of first phase in the heartwood segmentation, the estimated heartwood region was smoothed with morphological functions, such as dilation, erode and closing of OpenCV-library (Bradski, 2000). The heartwood region found with confidence connected region growing (Fig. 3e) was used as an input for the second segmentation phase performed with k nearest neighbor method.

2.4.2. K nearest neighbors (KNN) -matting in heartwood border adjusting

To adjust the border between the heartwood and sapwood regions, an image matting technique was applied based on k nearest neighbors (KNN) in matching non-local neighborhoods (Chen et al., 2013). The image matting process begins by dividing the image into three regions: foreground, background and unknown. These regions form an image

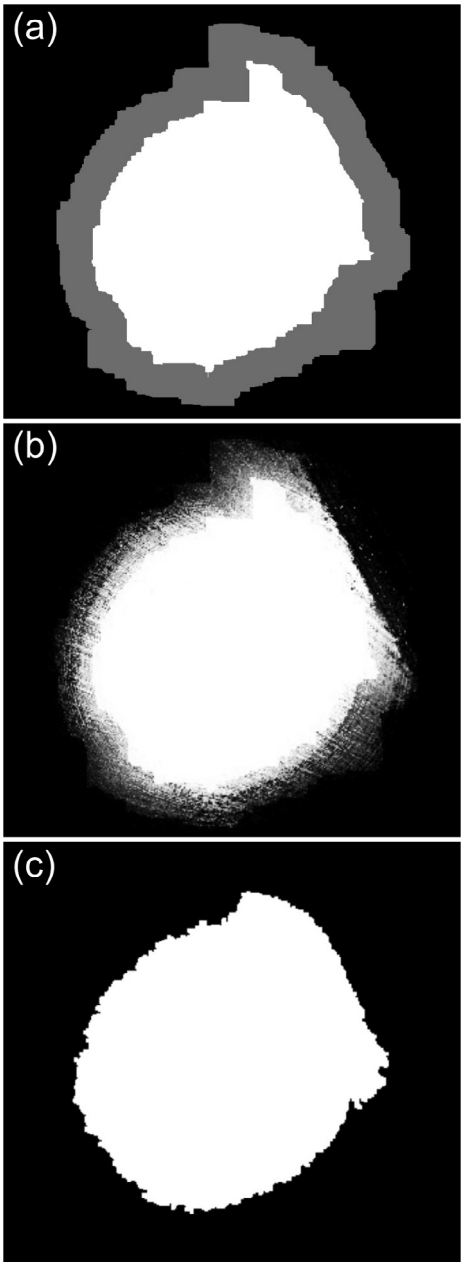

Fig. 4. KNN-matting of heartwood segment: (**a**) a coarse trimap of the log end face, (**b**) an alpha-layer, (**c**) the heartwood segment after the morphological functions.

called "trimap" (Fig. 4a). The drawing of the trimap was done automatically by the heartwood region border which was found in the first segmentation phase. Before the KNN-matting, the resolution of each study image was reduced significantly to 600 × 400 pixels to achieve faster computation of the images.

In our study, the estimated heartwood region forms a foreground in the trimap image (Fig. 4a). The unknown region of the trimap was drawn with a fixed width of 50 pixels from the edge of foreground region. The width of the unknown region was changed only if the edge of heartwood region was closer than 50 pixels to the background of image which made the unknown region to expand outside of the log end face. In this case, perimeter of the unknown region was set to 20 pixels apart from the edge of log end face. The limitation was made with an assumption that the heartwood does never reach a cambium layer of the wood (Uusitalo, 2004).

With the calculated trimap and the log end face image in HSV color space, the KNN-matting algorithm (Chen et al., 2013) defined a probability for each pixel in the unknown region to be included into heartwood region. The probability was based on matching the feature vectors between the known foreground and background and it was presented as an alpha matte (Fig. 4b). The alpha matte was then threshold with fixed value of 0.8, i.e., pixels with higher than 80% probability to be part of heartwood were chosen to the KNN-matte fine-tuned heartwood segment. The resulting binary image was processed (Fig. 4c) with morphological functions described in first phase of the segmentation algorithm.

When compared to the Fig. 3e, the resulting heartwood segment (Fig. 4c) follows the actual heartwood border more precise and the false spreading of the heartwood region in confidence connected region growing is reduced: error in estimated heartwood diameter decreased from 2.13 to −0.70 cm in the example (Fig. 3 and 4).

2.4.3. Diameter calculations from the log end face in polar coordinates

To evaluate the heartwood segmentation algorithm, the heartwood and the whole bottom end diameters were calculated for each algorithm segmentation (Fig. 4c), and its manually segmented ground-truth image (Fig. 2c). The segmentation images were transformed into polar coordinates (Fig. 5) according to the pith of the log end face. In the polar transformed image, the diameters were derived from intensity profiles of each column of the image. Position on the image y-axis where the pixel values changed from 255 (white) to 128 (gray), set a heartwood radii on each column of the image. Correspondingly, the log end face radii was found on the y-axis position where pixel values turned from gray to black (0). Yet, diameters were calculated by summing the opposing radii.

2.5. Experimental measurements

Experimental work was started by removing the plastic cover and the wood samples were measured by an impedance scanner in laboratory conditions. After a few days, the heartwood and sapwood region of the samples' cross-cut surfaces were detectable based on the color change. The position of the sapwood-heartwood border was based on a color and detected by a visual method with a bare eye. The heartwood content was determined from the north–south aspect of each sample using ruler with 1 mm resolution.

2.5.1. Impedance measurement system

The equipment consists of a control unit and a probe connected by cables with each other (Fig. 6). The measurement system consists of an

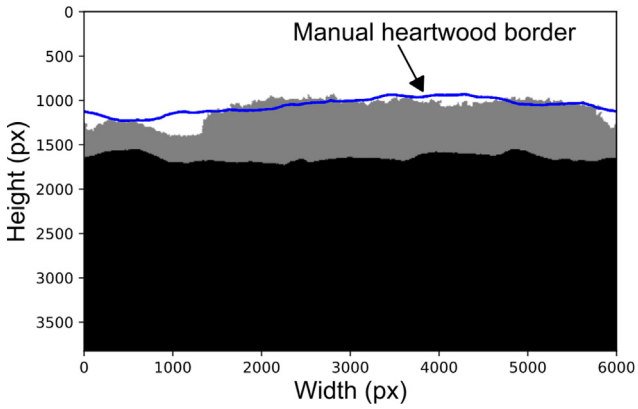

Fig. 5. A log end face image in polar coordinates (ϕ - r), according to the pith of the log end face. A white segment is the algorithm segmented heartwood. A blue line reaching across the polar image is the ground-truth heartwood border and an area in gray is the sapwood. (For interpretation of the references to colour in this figure legend, the reader is referred to the web version of this article.)

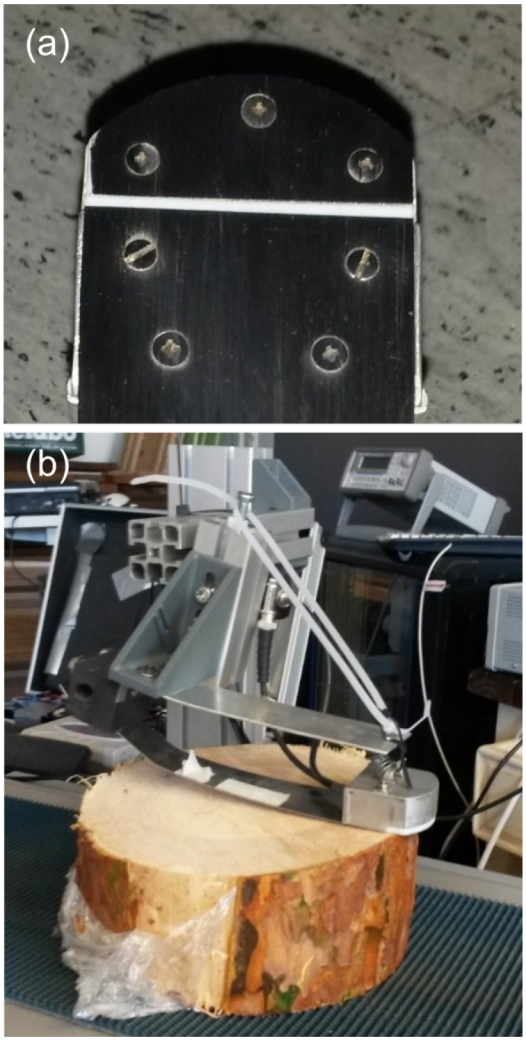

Fig. 6. (**a**) Scanning electrode configuration, the active electrode was 21 mm × 50 mm. Stainless steel electrodes were attached to 10 mm thick Teflon plastic sheet by screws. Gap between electrodes was 2 mm. (**b**) Impedance scanning measurement of cross-section, speed of the moving belt was 0.5 m/s. Coaxial cables (50 ohm) was used for the connections between electrodes and the impedance module.

impedance module, PC, ADC, DAC and a power card. The impedance module has connections for three signal wires (coaxial cables) and for the power wires. There is a measuring card with buffers, an adapter and connecting plugs for electrodes in the module. The software includes elements for testing the functioning of the equipment and calibration.

The impedance equipment is calibrated using open, short and lumped circuit corrections before the tests. Continuous or single measurements of spectrum can be made. In continuous measurement, a graph of impedance modulus is displayed on the PC screen. Detailed technical description of the impedance equipment may be found elsewhere (Tiitta and Olkkonen, 2002). When conducting continuous scanning measurements, the impedance electrodes were laid against the surface of wood (Fig. 6a). In the measurement, the impedance probe with stainless steel electrodes was placed in a holder. The used frequency was 40 kHz. Example of measured impedance is shown in Fig. 7.

2.6. Statistical analysis

Manual, image analysis and impedance measurements were analysed with an average heartwood diameter error and a paired samples t-test. In addition, the images produced by segmentation algorithm were

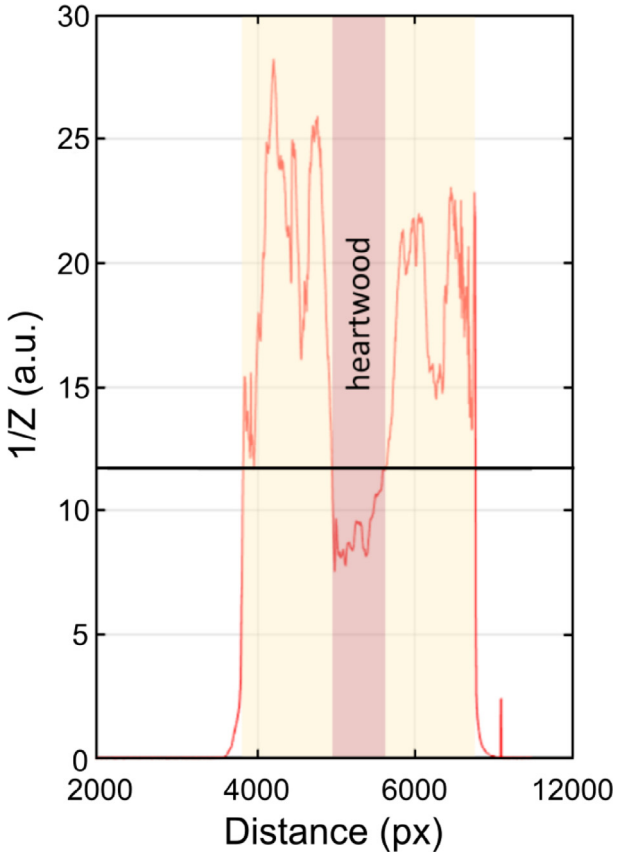

Fig. 7. Example of measured electrical impedance and heartwood as determined from the signal. The horizontal solid line is a threshold used for determining the borders.

compared to the ground-truth images with a Jaccard similarity index. Details about used methods are given in following sections.

2.6.1. Diameter analysis

The heartwood region segmented by the algorithm and heartwood average diameter were compared to ground-truth equivalents with a heartwood ratio error (IMG_{error}). The heartwood ratio error illustrates the relative error between the ground-truth and the algorithm acquired heartwood diameters and is calculated as follows

$$IMG_{error} = \left(\frac{HW_{DA} - HW_{DM}}{HW_{DM}}\right) \cdot 100, \tag{2}$$

where HW_{DA} and HW_{DM} stand for the heartwood diameters in pixels derived from the algorithm and the manual segmentations. In addition to the relative error described above, the heartwood diameter error was converted into the centimetres by scaling the pixel diameters by the measurement bar held in the original image.

The relative difference between EIS-measured and hand-measured heartwood diameter ratio was calculated as

$$EIS_{error} = \left(\frac{HW_{EIS} - HW_{Manual}}{HW_{Manual}}\right) \cdot 100, \tag{3}$$

where HW_{EIS} is the EIS-measured diameter of the heartwood within the log and HW_{Manual} is the heartwood diameter measured manually with a tape.

2.6.2. Shape comparison with similarity index

Jaccard index is well-known method to measure similarity between shapes. The index describes the size of an intersection divided by the size of a union of manual and algorithm segmentations. Jaccard index

Table 2
Average heartwood ratio results of each test set with paired t-test results. (Case I is manual vs. image, II: manual vs. impedance; III impedance vs. image.)

Case	Average Heartwood Ratio			Paired T-Test		
	Manual (Image)	Image analysis	EIS	t-value	df	p-value
I	0.608	0.581	–	2.42	85	0.017
II	0.507	–	0.554	3.17	32	0.003
III	–	0.556	0.602	−1.10	21	0.285

was defined as

$$J = \frac{S_M \cap S_A}{S_M \cup S_A}, \tag{4}$$

where S_M stands for the manually segmented area and S_A is the algorithm segmentation.

3. Results

The statistical difference between ground-truth, image analysis and EIS measured heartwood ratio was tested with a paired sample t-test. The t-test was carried out in three cases: (I) comparing the image analysis results to the ground truth (86 logs); (II) comparing the EIS measurement results to ground truth (33 logs); and III) comparing the image analysis results to the EIS measurement results for those logs that were measured with both methods (22 logs).

According to the paired t-test, the EIS was able to produce more reliable results than the image analysis (Table 2). The paired sample t-tests indicate that there were no statistical differences between the tested Case II where the impedance measurement results were compared with ground truth results. A p-value in the Case I indicated that there is slightly weaker, but statistically significant similarity between the image analyzed and manually measured heartwood ratios. The p-values in the Case III indicate that the results between EIS and image analyses vary significantly.

When analyzing the individual results from each test Case I and II, it can be seen that the image analysis produced systematic underestimations of the heartwood ratio (Fig. 8a) with an average error of −2.72% (−0.78 cm). Outcome of the image analysis segmentation was not affected by the ground-truth heartwood diameter ratio. The median value of IMG_{error} was −6.64% (−1.04 cm) which argues that data included such cases, where image analysis was unable to identify the intensity difference between heartwood and sapwood and produced considerable overestimations. Thus, the standard deviation within the IMG_{error} was also relatively broad, 20.02% (2.68 cm).

On the contrary, the EIS produced slight overestimations of the heartwood ratio in comparison to the ground truth values (Fig. 8a) and higher average heartwood diameter ratio error when compared to image analysis algorithm: an average EIS_{error} was 9.47% (1.28 cm) in the 33 log sample, median being slightly higher, 10.00% (1.40 cm). Again, this indicates that there were some outliers in data, which both methods were unable to capture. A standard deviation of the EIS_{error} was notable, 17.32% (2.25 cm). The diameter error estimates appear to be relatively normally distributed for both the image analysis and the EIS measurements (Fig. 9a and b).

The image analysis algorithm produced heartwood segments were compared to manual counterparts with Jaccard index. An average similarity between the segmentations was 0.81 which can be recognized as good segmentation result. The median value was slightly higher (0.85) because of the outliers where heartwood region was barely visible.

Combining the EIS and image analysis measurements (Fig. 8c) by calculating the average heartwood diameter ratio of the methods slightly decreased the heartwood ratio error. According to the Fig. 8c, the merged measurements are closer to diagonal line and have far less deviation (14.50%) than image analysis (IMG_{error} = 34.72%). However, the EIS derived heartwood diameter ratio has clearly lowest standard deviation (EIS_{error} = 12.59%) within the methods.

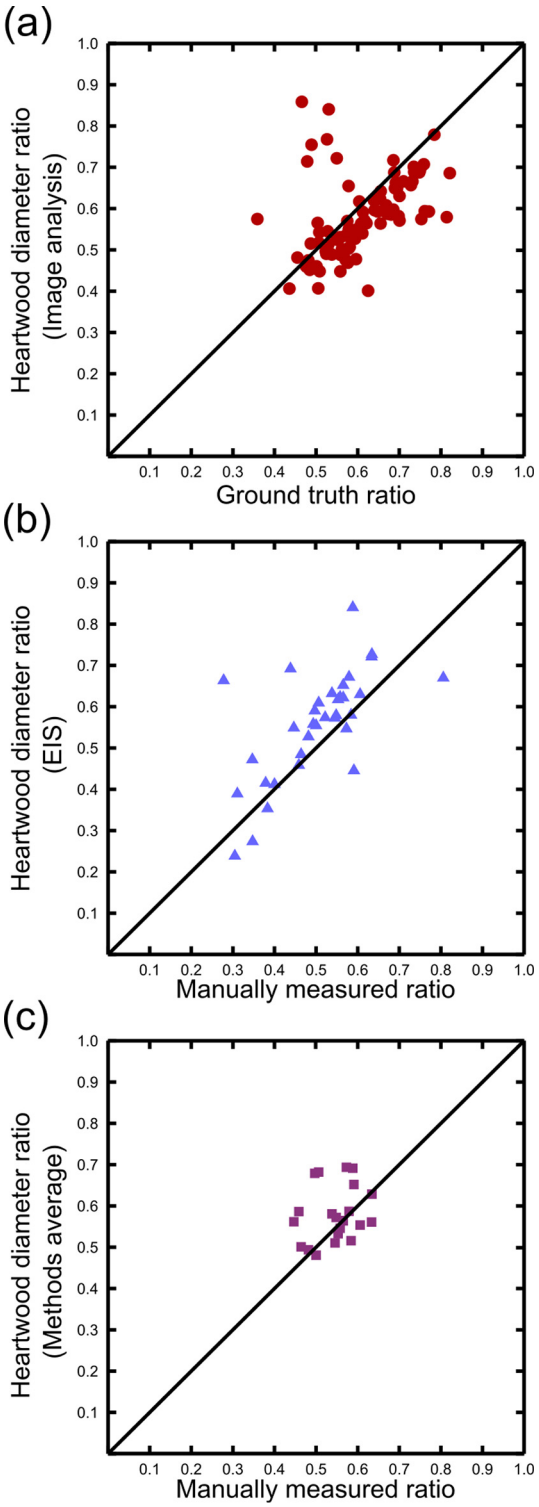

Fig. 8. Image analysis results (**a**) and EIS (**b**) of heartwood-stem diameter ratio compared with the ground truth results. (**c**) Case III (n = 22) presents a comparison of image analysis and EIS derived heartwood diameter ratios. Methods were combined by calculating average from the two estimates, which resulted the best outcome.

The average difference between combined heartwood ratio (image analysis and EIS) and hand-measured heartwood diameter ratio was

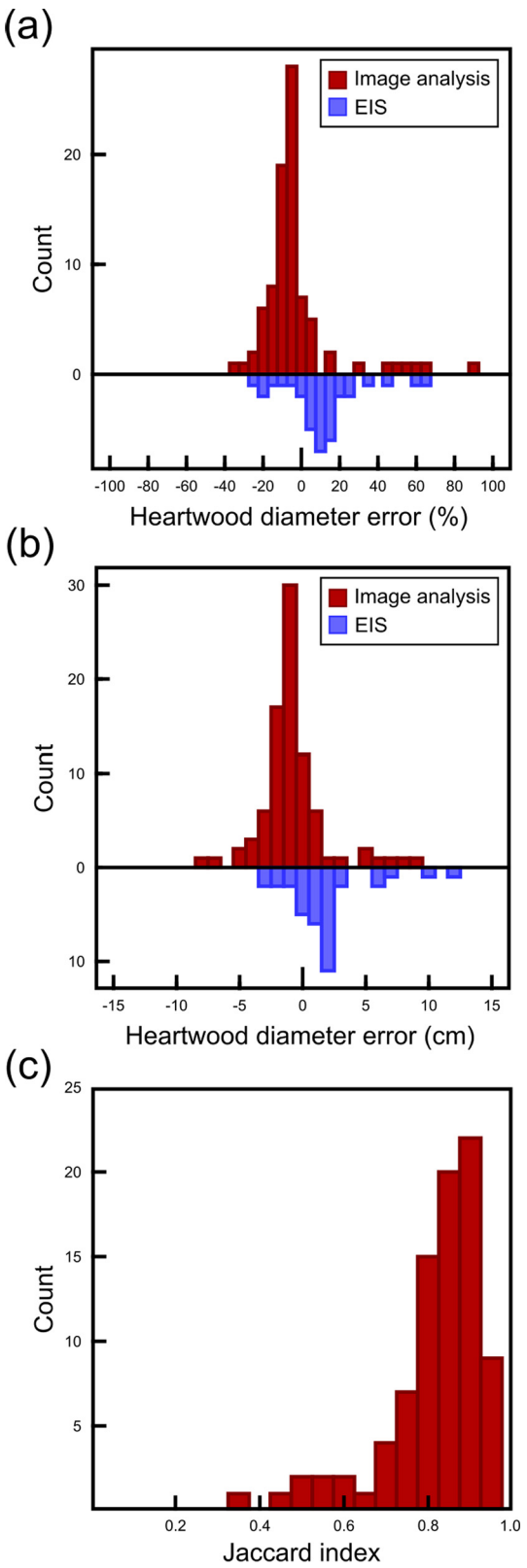

Fig. 9. Heartwood diameter error histograms for image analysis and EIS (**a**) Heartwood diameter error as percentage from manually measured heartwood diameter (IMG_{error}, EIS_{error}) (**b**) Error in centimeters (**c**) Similarity between manually and algorithm segmented heartwood.

6.78%, while error within image analyzed and EIS measured ratios was 8.91% and 10.24%. Due to the several large overestimations in the image analysis, the median of the error (−4.94%) is clearly below the average and diagonal (Fig. 8c). Therefore, combination of the methods had slightly lower average error in heartwood diameter ratio but clearly the lowest median error of 1.93%.

4. Discussion & conclusions

The statistical analyses indicate that the impedance measurement method was able to deliver more reliable results when comparing to the image analysis. Current results are fixed to the materials collected from two stands and more generalized results would require more comprehensive materials since the wood properties are known to vary between both stands and individual trees. Nevertheless, our test sites represented an average Scots pine harvesting conditions by age, soil fertility and tree size in Finland.

The t-test indicates that the impedance measurement system was more accurate than the image analysis-based method. However, the impedance measurement results were found to be overestimations comparing to ground truth manual measurements. These overestimations can be partially explained by analyzing the measurement systems and the heartwood formation mechanisms: impedance is measuring mainly the differences of moisture content whereas the manual measurement is based on the color changes due to variation of chemical structure in wood. The moisture content between the sapwood and heartwood is, although, transiting without clear boundary values before the chemical composition is changed in wood. Rust (1999) found out that the difference between low moisture content and chemically non-altered zone was approximately 0.4–2.5 cm in the Scots pine. Our results are parallel with this finding.

Both the image analysis and the EIS measurements were able to produce useful information from the wood raw material for industrial purposes. There is still potential to improve the methods and analyzes, for example hyperspectral cameras and optimized impedance electrodes can improve the results and therefore the usability of our findings even further. Though impedance spectra was measured, only one frequency was used in the main analyses here because the borders of sapwood and heartwood were clearly detectable with all the used frequencies. The electric field of lower frequencies differentiates from the electric field used in this study. The lower the frequency, the larger and more uneven field is generated inside the wood. Thus when detecting borders of electrically different regions, only the higher frequency was used to have as sharp response as possible. On the other hand, the lower frequencies may be used to improve the impedance analyses because of the different polarization mechanism than with the highest frequencies.

Extending the initial region growing based segmentation with the KNN-matting improved the heartwood diameter estimations significantly: the relative difference between manually determined heartwood diameter and algorithm calculated diameter was reduced over 10% and the similarity between segments was increased by 5% with the KNN-matting. An increased segmentation accuracy does come at cost of a increased computation time. Thus, it's debatable whether KNN-matting could be performed in an operational bucking without a notable investments into on-board computing hardware.

Practical applications in mind, a deep learning with convolutional neural networks to detect the heartwood from the log end face image should be investigated in the future research. Yet, finding a solution to extract the background from the log end face image was not discussed in this study because the lightning and the background of a image would be different in an actual device mounted on a harvester head. To extract the background of the log end face image in harvester application, a robust, color histogram-based segmentation (Riehle et al., 2020) could be considered.

The heartwood diameter error in the image analysis was exceptionally high with log end faces where the disparity between heartwood and sapwood was low. In some situations, when the outer bark of tree was thick, the bark was pulverized during the cutting and chainsaw conveyed the fine dust on the cross-cut surface. The dust

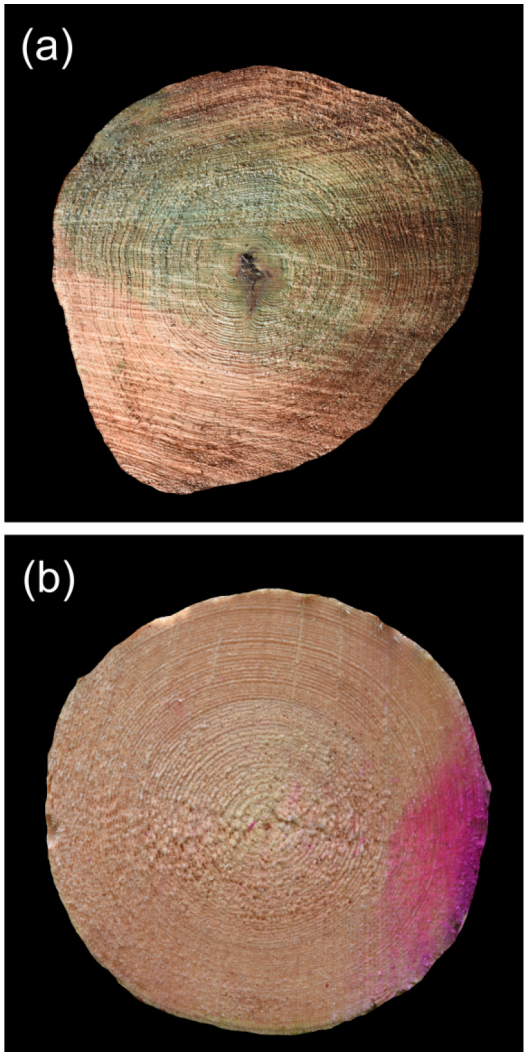

Fig. 10. Examples of the log end images where the heartwood segmentation algorithm did not succeed. (**a**) IMG_{error} = 54.6% (8.4 cm), J = 0.53 (**b**) IMG_{error} = 88.5% (9.0 cm), J = 0.36. Red color in (**b**) is marker color of the harvester. (For interpretation of the references to colour in this figure legend, the reader is referred to the web version of this article.)

covered the log end and thus detailed image analysis was very difficult to perform (Fig. 10).

Even though the tests were carried out during a summertime, it can be expected that both the image analysis and the impedance-based systems will work during a wintertime because then the moisture content of sapwood is generally higher than during the growing season. The increased difference of moisture content between the heartwood and the sapwood can be detected due to higher variation in both visual appearance and in electrical conductivity. Furthermore, winter conditions may prevent the fine bark dust from adhering to the cross-cut face of the log which would improve the usability of the image analysis. Yet, the harsh outdoor conditions due to varying humidity and sunlight together with a vibration of the harvester, can cause challenges to the adaptation of a camera technology to a harvester head.

After all, these results suggest that the image analysis can be executed when quality of log end face images is at least decent. This has also been confirmed by other studies of this field (Norell and Borgefors, 2008; Schraml et al., 2015), where coarse log end face images were used in image analysis. In our study, the log end faces were practically as fresh as the log would be at the moment of cross-cut made by the harvester which makes image analysis more difficult than in a case where logs have dried out. However, the image analysis is only suitable in cases where the heartwood region can be visually interpret from log end and in order to evaluate the true suitability of both methods in harvesting tests with a larger sample size with a seasonal variation is encouraged.

Findings of this study indicate that both studied novel methods show potential to measure heartwood in the harvesting phase and further optimize the raw material flows with the obtained information. If the utilization of Scots pine heartwood would be maximized in the wood value chains, the information received from the EIS and the image analysis should be adapted in the tree bucking. This adaptation will eventually require information about the absolute and relative values of heartwood products which should be further investigated. The utilization of heartwood will most likely increase in the future because of the high natural durability against weather and fungi.

CRediT authorship contribution statement

Antti Raatevaara: Methodology, Software, Validation, Formal analysis, Writing - original draft, Visualization. **Heikki Korpunen:** Methodology, Validation, Formal analysis, Investigation, Writing - original draft, Supervision, Project administration. **Markku Tiitta:** Methodology, Validation, Formal analysis, Investigation, Writing - original draft, Visualization, Project administration, Funding acquisition. **Laura Tomppo:** Methodology, Validation, Formal analysis, Investigation, Writing - original draft, Visualization, Project administration, Funding acquisition. **Sampo Kulju:** Methodology, Software, Validation, Formal analysis, Writing - original draft, Visualization. **Jukka Antikainen:** Methodology, Software, Validation, Formal analysis, Investigation, Funding acquisition. **Jori Uusitalo:** Conceptualization, Formal analysis, Writing - review & editing, Supervision, Project administration, Funding acquisition.

Declaration of Competing Interest

The authors declare that they have no known competing financial interests or personal relationships that could have appeared to influence the work reported in this paper.

Acknowledgements

The study was funded by Business Finland (EURA2014, Grant No. A72280), as well as Ponsse Plc., UPM-Kymmene Corporation, Metsä Group, Trimble Inc. and Metsämiesten Säätiö Foundation.

Appendix A. Supplementary material

Supplementary data associated with this article can be found, in the online version, at https://doi.org/10.1016/j.compag.2020.105690.

References

Arshadi, M., Backlund, I., Geladi, P., Bergsten, U., 2013. Comparison of fatty and resin acid composition in boreal lodgepole pine and Scots pine for biorefinery applications. Ind. Crop. Prod. 49, 535–541. https://doi.org/10.1016/j.indcrop.2013.05.038.

Barsoukov, E., Macdonald, J.R., 2005. Impedance spectroscopy: theory, experiment, and applications. John Wiley & Sons, pp. 616. https://doi.org/10.1002/9781119381860.

Björklund, L., 1999. Identifying heartwood-rich stands or stems of Pinus sylvestris by using inventory data. Silva Fenn. 33, 119–129. https://doi.org/10.1016/j.jchb.2015.06.005.

Bradski, G., 2000. The OpenCV library. Dr. Dobb's J. Software Tools 25, 122–125.

Chen, Q., Li, D., Tang, C.K., 2013. KNN matting. IEEE T. Pattern Anal. 35, 2175–2188. https://doi.org/10.1109/TPAMI.2013.18.

Gazo, R., Vanek, J., Abdul_Massih, M., Benes, B., 2020. A fast pith detection for computed tomography scanned hardwood logs. Comput. Electron. Agr. 170, 105107. doi:10.1016/j.compag.2019.105107.

Harju, A.M., Venäläinen, M., Anttonen, S., Viitanen, H., Kainulainen, P., Saranpää, P., Vapaavuori, E., 2003. Chemical factors affecting the brown-rot decay resistance of Scots pine heartwood. Trees-Struct. Funct. 17, 263–268. https://doi.org/10.1007/

S00468-002-0233-Z.
Kapur, J.N., Sahoo, P.K., Wong, A.K.C., 1985. A new method for gray-level picture thresholding using the entropy of the histogram. Comput. Vision, Graph., Image Process. 29, 273–285. https://doi.org/10.1016/0734-189X(85)90125-2.
Lowekamp, B.C., Chen, D.T., Ibáñez, L., Blezek, D., 2013. The design of SimpleITK. Front. Neuroinform. 7, 45. https://doi.org/10.3389/fninf.2013.00045.
Nagy, N.E., Krokene, P., Solheim, H., 2006. Anatomical-based defense responses of Scots pine (Pinus sylvestris) stems to two fungal pathogens. Tree Physiol. 26, 159–167. https://doi.org/10.1093/treephys/26.2.159.
Nascimento, M., Santana, A.L.B.D., Maranhão, A., Oliveira, L., Bieber, L., 2013. Phenolic Extractives and Natural Resistance of Wood, in: Biodegradation - Life of Science. InTech. volume 2, pp. 349–370. doi:10.5772/56358.
Natural Resources Institute Finland, 2019. E-yearbook of Food and Natural Resource Statistics for 2018. Natural resources and bioeconomy studies 30/2019. p. 105.
Norell, K., 2011. Automatic counting of annual rings on Pinus sylvestris end faces in sawmill industry. Comput. Electron. Agr. 75, 231–237. https://doi.org/10.1016/j.compag.2010.11.005.
Norell, K., Borgefors, G., 2008. Estimation of pith position in untreated log ends in sawmill environments. Comput. Electron. Agr. 63, 155–167. https://doi.org/10.1016/j.compag.2008.02.006.
Riehle, D., Reiser, D., Griepentrog, H.W., 2020. Robust index-based semantic plant/background segmentation for RGB- images. Comput. Electron. Agr. 169, 105201. https://doi.org/10.1016/j.compag.2019.105201.
Royer, M., Houde, R., Viano, Y., Stevanovic, T., 2012. Non-wood Forest Products Based on Extractives - A New Opportunity for the Canadian Forest Industry Part 1: Hardwood Forest Species. J. Food Res. 1, 8. https://doi.org/10.5539/jfr.v1n3p8.
Rust, S., 1999. Comparison of three methods for determining the conductive xylem area of Scots pine (Pinus sylvestris). Forestry 72, 103–108. https://doi.org/10.1093/forestry/72.2.103.
Schraml, R., Charwat-Pessler, J., Petutschnigg, A., Uhl, A., 2015. Towards the applicability of biometric wood log traceability using digital log end images. Comput. Electron. Agr. 119, 112–122. https://doi.org/10.1016/j.compag.2015.10.003.
Tiitta, M., 2006. Non-destructive methods for characterisation of wood material. Ph.D. thesis. University of Kuopio.
Tiitta, M., Kainulainen, P., Harju, A.M., Venäläinen, M., Manninen, A.M., Vuorinen, M., H.Viitanen, H., 2003. Comparing the effect of chemical and physical properties on complex electrical impedance of scots pine wood. Holzforschung 57, 433–439. https://doi.org/10.1515/HF.2003.064.
Tiitta, M., Olkkonen, H., 2002. Electrical impedance spectroscopy device for measurement of moisture gradients in wood. Rev. Sci. Instrum. 73, 3093–3100. https://doi.org/10.1063/1.1485783.
Tiitta, M., Tiitta, V., Heikkinen, J., Lappalainen, R., Tomppo, L., 2020. Classification of Wood Chips Using Electrical Impedance Spectroscopy and Machine Learning. Sensors 20, 1076. https://doi.org/10.3390/s20041076.
Tiitta, M., Tomppo, L., Möttönen, V., Marttila, J., Antikainen, J., Lappalainen, R., Heräjärvi, H., 2017. Predicting the bending properties of air dried and modified Populus tremula L. wood using combined air-coupled ultrasound and electrical impedance spectroscopy. Eur. J. Wood Wood Prod. 75, 701–709. https://doi.org/10.1007/s00107-016-1140-0.
Tomppo, L., Tiitta, M., Laakso, T., Harju, A., Venäläinen, M., Lappalainen, R., 2011. Study of stilbene and resin acid content of Scots pine heartwood by electrical impedance spectroscopy (EIS). Holzforschung 65, 643–649. https://doi.org/10.1515/hf.2011.111.
Uusitalo, J., 2004. Heartwood and extractive content of Scots pine in Southern Finland: Models to apply at harvest. Wood Fiber. Sci. 36.
Zelinka, S.L., Rammer, D.R., Stone, D.S., 2008. Impedance spectroscopy and circuit modeling of Southern pine above 20% moisture content. Holzforschung 62, 737–744. https://doi.org/10.1515/HF.2008.115.